Published in final edited form as:
Nanomedicine. 2013 November ; 9(8): . doi:10.1016/j.nano.2013.04.011.

Ultrabright Fluorescent Mesoporous Silica Nanoparticles for Prescreening of Cervical Cancer

Shajesh Palantavida, Ph.D.[1], **Nataliia V. Guz, M.S.**[1], **C.D. Woodworth, Ph.D.**[2], and **I. Sokolov, Ph.D.**[1,2,3]

[1]Department of Mechanical and Biomedical Engineering, Tufts University, Medford, MA 01255, USA

[2]Department of Physics, Clarkson University, Potsdam, New York 13699-5820, USA

[3]Department of Biology, Clarkson University, Potsdam, New York 13699-5820, USA

[4]Nanoengineering and Biotechnology Laboratories Center (NABLAB), Clarkson University, Potsdam, New York 13699-5820, USA

Abstract

We report on the first functional use of recently introduced ultrabright fluorescent mesoporous silica nanoparticles, which are functionalized with folic acid, to distinguish cancerous and precancerous cervical epithelial cells from normal cells. The high brightness of the particles is advantageous for fast and reliable identification of both precancerous and cancerous cells. Normal and cancer cells were isolated from three healthy women and three cancer patients. Three precancerous cell lines were derived by immortalization of primary cultures of normal cells with human papillomavirus type-16 (HPV-16) DNA. We observed substantially different particle internalization by normal and cancerous/precancerous cells after a short incubation time of 15 minutes. Compared to HPV-DNA and cell pathology tests, which are currently used for prescreening of cervical cancer, we demonstrated that the specificity of our method was similar (94-95%), whereas its sensitivity was significantly better (95-97%) than the sensitivity of those currently used tests (16%-82%).

Keywords

cervical cancer; early cancer detection; novel detection methods; fluorescent silica particles; Pap smear/liquid cytology tests

Corresponding author: Igor Sokolov, Departments of Mechanical and Biomedical Engineering, 204 Anderson Hall, Tufts University, Medford, MA 01255, USA; Phone: 1-617-627- 2548; Fax: 1- 617-627-3058, igor.sokolov@tufts.edu.

The authors have no conflicts of interest to declare.

Supporting Information **Available**: The particle synthesis, characterization, and detailed statistics of fluorescent intensities of normal, cancer, and precancerous cells internalized with SI-AF1 and SI-AF2 fluorescent silica nanoparticles

Introduction

Cervical cancer is the second most common cause of cancer death in women worldwide, and infection with oncogenic human papillomavirus (HPV) is the most significant risk factor in its aetiology.[1] The mortality rate is second only to that for breast cancer. Early detection of cervical cancer can substantially decrease mortality. Early detection is based on identifying neoplastic cells in stained preparations obtained from the uterine cervix. The cytological tests performed by pathologists **(**Pap smear and liquid-based cytology[2]) are relatively simple and minimally invasive (the cells are obtained from the cervix using a combination of a spatula and brush). Despite the impressive success of cervical cytology, its sensitivity for detecting preinvasive cervical lesions is far from desirable, with mean sensitivity of only 47% (range 30 - 80%). The sensitivity of the cytological tests for invasive carcinoma is also not perfect, ranging from 16% to 82% in different studies.[3, 4] Such a low accuracy can be explained by inherent problems with identifying neoplastic cells with cytological test methodology. For example, there are multiple benign mimics of neoplastic cells such as atypia of repair, atrophy, radiation change, effect of intrauterine device, and metaplasia. When these cells are encountered, additional testing for HPV DNA and/or colposcopy and biopsy[5], is required, substantially increasing the cost and resulting in more invasive evaluation. According to the American Cancer Society, each year in the United States alone approximately 3.6 million cytological tests are classified as equivocal, out of which only 8% of women will have preinvasive (high-grade squamous intraepithelial) lesions, and only 0.4% will have carcinoma as found through further testing that involves invasive tissue biopsies. Thus, more accurate cytological tests may substantially decrease the cost and patient inconvenience of screening by eliminating additional steps of HPV DNA testing and colposcopy with biopsy.

The economic constraints in developing countries have prompted alternative methods of screening for cancer including visual inspection after application of 3-5% of acetic acid[6] and Lugol's iodine[7]. The major disadvantage of these tests is low specificity. Given the considerable variation in the way these tests are applied and interpreted in different settings, there is no standard universally accepted definition of the test results. It remains to be seen if the specificity can be improved by further developments in test definitions and training strategies. The inability of these test methods to unambiguously detect abnormal cells during the early stages poses a major challenge in an effort to reduce mortality associated with cervical cancer.

Demands for the development of a universal testing and screening method have generated a large scientific and industrial interest. Optical techniques like fluorescent microscopy, confocal imaging[8] and optical coherence tomography (OCT)[9] have shown promise for cervical precancer detection as measured against the traditional methods such a Pap smear. The sensitivity and specificities of these optical techniques have been reported to reach 80-90% in small and moderate clinical trials.

Targeting particle probes is the topic of considerable interest for applications in cancer diagnostics and therapeutics.[10-13] Cancer-specific nanoparticles can further be used for targeting drug delivery thereby improving the therapeutic efficacy and reducing side effects of chemotherapeutic drugs. [14] Targeting nanoparticles have been demonstrated for the use as suitable imaging agents in noninvasive tumor imaging[15], and for diagnosis and delineation of tumor margins during surgical resectioning. Specific cancer targeting is achieved by functionalizing the nanoparticles with ligands specific to cell receptors overexpressed in cancer cells. Folic acid[16], SV119[17], and cRGDY peptide[18] are examples of ligands that can impart specificity to nanoparticles and specifically target folate, $\alpha_v\beta_3$ integrin and sigma 2 receptors of cells, respectively. Folite-receptor mediated targeting has been broadly

investigated in specific tumor targeting.[12, 19] Many forms of carcinoma, such as ovarian, lung, breast, kidney, brain, endometrium, and colon cancers overexpress folic acid receptors. The expression of this receptor in malignant tissues can exceed that in normal tissues by two orders of magnitude.[20] Hence, folate targeting may also prove effective in diagnosing epithelial cancers at an earlier stage. A preferential internalization of folic acid functionalized nanoparticles by malignant cells can form a diagnostic test for detection of the disease. Even though the reported literature on the folic acid functionalized particles suggests such applications, there have been only a few investigations of cervical cancer cells.[21-24] Only one work dealt with several cell lines. [22] Thus, there is a need to study the interaction between folite-functionalized particles and a model relevant to the clinical tests for prescreening of cervical cancer. Such a model should include both cancerous and precancerous (immortalized), as well as normal cervical cells. This is done in the present work.

Recently, a new type of mesoporous silica particle was reported that physically encapsulates fluorescent dye molecules in the pore channels. These nanoparticles effectively encapsulated the dye without leakage or aggregation of the dye molecules up to very high concentration of the dye inside the particles. This results in unusually high fluorescent brightness termed ultrabrightness.[25-28] As an example, a ~40 nm ultrabright silica nanoparticle has a dye concentration of 0.03M, which is almost four orders of magnitude higher than the maximum concentration of the dye without fluorescent quenching in water (~4μM). In order to exploit the high brightness for targeting of cervical cancer, the particles should be functionalized with folic acid. This is a rather challenging task because it requires organic solvent, which can effectively wash the dye out of the particles. We have recently solved this challenge through intermediate amine functionalization.[29] The folic acid conjugation steps reduced the amount of the dye encapsulated in the particles. Nevertheless they were substantially brighter than the probes of similar sizes reported previously.

There is a general significance in demonstrating the labeling ability of highly fluorescent nanoparticles. When studying the interaction between folite-functionalized nanoparticles and cells, the internalization times used in most of the reported literature are about several hours, and can reach even several days. This may be a serious disadvantage when detecting specific cells, for example, leukemia cells [30], in particular *in-vivo*. The high brightness of functionalized fluorescent particles will help to yield a significant fluorescence contrast between (pre)cancerous and normal cells in a shorter incubation time. This also implies that only low concentrations of nanoparticles will be required for effective detection, which is important for *in-vivo* applications.

Here we report on the use of ultrabright fluorescent silica nanoparticles functionalized with folic acid to label cervical epithelial cells. The cell model used was chosen to analyze the potential clinical value of the labeling method. After internationalization of the fluorescent particles, the cells were imaged with a fluorescent optical microscopy. Fluorescence microscopy is a fast and cost-effective procedure for disease surveillance and diagnosis in hospital and outpatient care.[31] To mimic the clinical prescreening tests for cervical cancer (Pap smear and liquid-based cytology), the following cell model was used here: primary normal, precancerous (immortalized), and cervical carcinoma cells. The normal and carcinoma cells were extracted from issues of three healthy patients and patients with cervical cancer. Three precancerous cell lines were derived by immortalization of primary normal cells with human papillomavirus HPV-16. Folic acid functionalized particles obtained through two different approaches were used in this study. We observed the specificity of our method to be similar (94-95%) to the existing HPV DNA and cell pathology tests, which are currently used for prescreening of cervical cancer. At the same

time, the sensitivity of the described method was significantly better (95-97%) than sensitivity of the currently used tests (16%-82%).

Methods

Ultrabright mesoporous silica nanoparticles functionalized with folic acid

The synthesis of ultrabright fluorescent silica nanoparticles is described in [27, 28]. The particles were substantially brighter than quantum dots of similar spectral characteristics (with the fluorescent maximum of 545nm was exciting with either 488 or 525nm). Amine groups were introduced through introduction of a co-silica source (aminoporpyltriethoxysilane). [29] In order to obtain folic acid functionalized nanoparticles two approaches were used. In a precursor modification approach, the amine precursor was modified by conjugation to folic acid, prior to co-condensation with inorganic silica precursor, achieved during nanoparticle synthesis. This sample is labeled as SI-AF1. In the surface grafting approach, amine modified nanoparticle (obtained by co condensation of amine precursor with inorganic silica precursor) sol was stirred for 3 h at room temperature with a premixed solution containing folic acid. This sample is labeled as SI-AF2. The details of the synthesis are described in the Supplementary Materials.

Cell model

HPV-associated cervical carcinogenesis is a multistep process leading to the transformation of the infected cells to pre-malignant cells (or cervical intraepithelial neoplasia) CIN.[32] The cells associated with the lesions become atypical and mitotically active, become immortal, and they are characterized by the inability to terminally differentiate.[33] Here we compare a cell model comprising normal, immortalized (pre-malignant), and carcinoma (cancer) cells.

Primary cultures of human cervical epithelial cells were prepared by a two-stage enzymatic digestion of cervical tissue as described.[34] Briefly, all human tissues were obtained from the Cooperative Human Tissue Network. Informed consent was obtained from patients according to their published guidelines (http://chtn.nci.nih.gov/phspolicies.html). Each tissue was digested for 16 hours at 4°C in dispase. Then, the layer of epithelial cells was removed from the underlying connective tissue by scraping. The sheet of epithelial cells was cut into 1mm^2 pieces and digested in 0.25% trypsin at 37°C for 10 minutes. Trypsin was neutralized by adding fetal bovine serum. The cells were collected by low speed centrifugation. Cultures consisting of ≥ 95% epithelial cells were maintained in keratinocyte serum-free medium (Invitrogen) which prevents outgrowth of fibroblasts and other stromal cells. HPV-16 immortalized cell lines[35] and cervical carcinoma cell lines[36] were also maintained in KSFM and no evidence of contamination by fibroblasts or other stromal cells was observed.

The immortalized (pre-malignant) cell lines were prepared in two steps: 1) transfection of normal cervical cells with the complete HPV-16 genome, and 2) subsequent immortalization of the transfected cells. HPV genes were introduced into cultured cervical cells by transfection with plasmid DNA containing the complete HPV-16 genome in combination with the neomycin resistance gene [34]. Subsequently, medium was changed and cells grew for 24 hours before cultures were split 1:3. After 24 hours, transfected cells were selected by growth for 2 days in KSFM containing 200μg/ml G418 and used immediately. Only immortalized cells survived after 60-70 population doublings (PDs). Normal cervical cells were used between 40 to 60 PDs, and carcinoma cell lines were used at 90 to 120 PDs. The slightly higher number of PDs for (pre)cancer cell lines avoids potential confusion because any normal cells (epithelial cells or stromal cells) that may contaminate the cancer culture dishes would die out by that number of PDs.

Cancerous CXT-1, 2 and 7, precancerous CX 16-1, 16-2 and 18-3 cell lines and normal HCX-132, 162 and 397 strains were used here. For the imaging study, all cells were cultured in two-welled Lab-Tek slides (Thermoscientific). The cells were used for experiments when the cells were not more than 60-80% confluent. The cells were washed with phosphate buffered saline (PBS) prior to incubation with nanoparticles. Incubation with each nanoparticle suspension was done for 15 min (1mL of particles in PBS in concentration of 9.3×10^{13} particles/L was added to cells). To remove unbound/not internalized particles, cells were washed twice with PBS, and used for the imaging right after that.

Characterization

A C1 Eclipse Nikon TE2000U fluorescent confocal microscope was used to collect fluorescent images of cells. A blue argon ion laser with a wavelength of 488 nm was used for excitation of fluorescence. The optical gains for both channels were 8.40 and the dwell time was 6.48μs for all measurements. A 60× objective was used for the imaging. A medium pinhole was used. A pixel resolution of 512×512 was set to acquire the images.

Particle size distributions and zeta-potential measurements were obtained using a dynamic light scattering (DLS), particle-size analyzer (Brookhaven, NY) equipped with a standard 35 mW diode laser and an avalanche photodiode detector. 0.25 ml of stock solution (as synthesized) was diluted to 3 ml with deionized water and ultrasonicated for 5 min prior to the DLS measurements. The most probable diameters presented are averages of three runs. A fluorescence spectrophotometer (Varian, Cary Eclipse), and a UV-2401PC UV–Vis spectrophotometer (Shimadzu, Japan) were used to control the fluorescent brightness of the particles.

Results

The most abundant particle size obtained from the DLS measurements was 75nm for SI-AF1 and 46 nm for SI-AF2 particles. The zeta potential measurement of SI-AF1 particles yielded values around zero (in the range -2 and 2 mV for different runs). SI-AF2 particles showed the values of zeta potential of − (15 ± 3) mV.

The fluorescent brightness of the particles was calculated relative to the brightness of single molecule of encapsulated dye, rhodamine 6G (R6G) as described in refs. [37, 38] in detail. Following this method, we can find that SI-AF1 particles have the brightness equivalent to 2200 ± 200 R6G dye molecules, whereas SI-AF2 particles had brightness equivalent to 200 ± 50 R6G dye molecules.

Representative fluorescent confocal images of cancer, precancerous, and normal cells after incubating with particles for 15 minutes are provided as Figure 1. To quantify the amount of internalization, which is proportional to the fluorescence of cells, the average fluorescent pixel intensity of each cell was calculated from the fluorescent images of cells. About 100 cells of 20 different images were analyzed for each cell and particle type. The background pixel intensity was also measured for the areas free of cells. The background intensity per pixel was found to be in the range 35 – 45 arbitrary units (au) for all images analyzed irrespective of the cell and particle types. This independently confirms the uniformity of the imaging conditions for the images analyzed. To exclude the background intensity from the calculation, only the pixel intensities above 50au were counted towards the cell fluorescence. Cell internalization studies have shown that the internalized particles are mostly aggregated inside vesicles and vesicles are distributed in the cytoplasm.[39] This in turn leads to a non-uniform distribution of particles within the cell and the presence of the background pixels in the cell images. Therefore, the *average* pixel intensity per cell has been calculated.

Histograms of average pixel intensity of normal, cancer, and precancerous cells are provided as Figure 2. Descriptive statistics of the distributions shown in Figure 2 is provided in Supplementary Materials as Table S1. Cancer and precancerous cells have higher average pixel intensities than normal cells irrespective of the type of particles used. The use of SI-AF2 particles results in a higher proportion of cells acquiring higher average intensity in the case of cancer and precancerous cells. There is some overlap of distributions for normal and the other cell types which prevents unambiguous separation of cells.

Box plots of average pixel intensity per cell obtained for all cell cultures treated with SI-AF1 and SI-AF2 particles are provided as Figure 3. (The box plot for each subject separately is provided in Supplementary Materials as Figure S1.) One can quantitatively see that the majority of cancer cells are brighter than normal cells. Precancerous cells have the intensities similar to that of cancer cells. Cancer cells have a broader distribution of average florescent intensities compared to normal cells. Segregation between intensities for cancer, precancerous and normal cells increases when using SI-AF2 particles. The number of cells having average pixel intensity higher than 100 is much less for normal cells for both type of particles.

Statistical analysis of the observed differences is done by using the Mann Whitney U tests. [40] The nonparametric tests were chosen because of essentially non-Gaussian distributions seen in Figure 2. The sample sizes in the Mann Whitney tests were ~300. The U values and the significance p (one tailed) up to which the groups differed significantly are shown in Table 1. One can see that the differences between normal cells and either cancer or precancerous cells are statistically significant for $p<0.0001$. At the same time, the cancer and precancerous distributions were not significantly different. A similar behavior was observed in the case of SI-AF1 particles.

To understand the potential clinical relevance of our results, we calculate receiver operating characteristic (ROC) curves.[41, 42] The ROC curves were calculated for cancer – normal and normal– precancerous groups. When a threshold for the average pixel intensity is specified, the classification of cells into normal and malignant is possible. If the fluorescent intensity of a cell is above the threshold, the cell is classified as malignant. The efficiency of the test to distinguish a cancer, precancerous, and normal cell can be represented in the form of the ROC curve. For an example of cancer vs normal cells, all cancer cells with intensity above the specified threshold value will be a true positive outcome, and every cancer cell below the threshold will be a false negative outcome. Similarly, every normal cell above the threshold will be a false positive outcome, and every normal cell below the threshold will be a true negative outcome. The ROC curves obtained are provided as Figure 4.

Discussion

The particles synthesized can be called ultrabright because of their high fluorescent brightness which was presented in the Results section. It could be compared with bright quantum dots emitting fluorescent light in the same part of the spectrum. As an example, a highly (green) fluorescent CdSe/ZnS quantum dot is ~20 times brighter than green organic fluorophore, rhodamine 6G. [43, 44] This means that the fluorescent brightness of SI-AF1 particles is equivalent to 110 CdSe/ZnS quantum dots, whereas SI-AF2 particles had brightness equivalent to 10 quantum dots.

Zeta potentials of the synthesized particles indicate the presence of folic acid on the particle's surface. Disassociation/ionization of the α-carboxyl group on folic acid imparts a negative charge to the particle surface. Hence, the lower negative value for SI-AF2 particles should indicate a higher folic acid group density on the particle surface compared to SI-AF1

(note that the particles with no folites show positive zeta potential due to amine groups [29]). Covalent linking of folic acid through its γ-carboxyl to a substrate does not affect its binding affinity to the folic acid receptor and endocytosis proceeds unhindered through the receptor mediated pathway.[45] The enhanced internalization of folate functionalized fluorescent silica nanoparticles seen in Figure 1 for cancerous and precancerous cells indicates that a substantial part of folic acid was linked through its γ-carboxyl group, leaving α-carboxyl group active. Furthermore, because SI-AF2 particles are less bright than SI-AF1 ones, this implies substantially higher internalization with SI-AF2 particles compared to SI-AF1 ones. Since SI-AF2 particles have more folite molecules attached, it suggests that the mechanism of uptake is mediated by the folic acid receptor.

A noticeable difference in fluorescence between cancer and normal cells required many hours of incubation when using regular fluorescent folite taggants. [12, 19] A significant fluorescence acquired by cells within a short 15-min incubation time can be explained by the high brightness of the nanoparticles.

A careful visual observation shows that normal cells have also acquired some fluorescence. Nonspecific uptake of the particles by cells is well reported. It is known that the rate of nonspecific uptake of nanoparticles depends on their size.[39, 46, 47] The nanoparticles used in this study are in the size range where some nonspecific uptake was observed. A smaller amount of folic acid receptor on normal cells also contributes to the internalization of normal cells with the folite-functionalized nanoparticles. It is also interesting that higher fluorescence intensity is observed for HCX 397 compared to HCX 162. Obviously, there is variability in the behavior of cells towards internalization of nanoparticles.

When analyzing the ROC curves, one can note that the curves shown in Figure 4 cover a high area for both types of particles, which means high efficiency of such tests. In the case of SI-AF1, the maximum of the Youden index was obtained for the threshold of 106 when the corresponding sensitivity and specificity were 93% and 88%, respectively. In the case of SI-AF2 particles this maximum was at the threshold of 110 when the corresponding sensitivity and specificity were 95% and 94%, respectively. The area under the curve for SI-AF1 particle was 0.960 and that of SI-AF2 was 0.985. (The area under a perfect test will be 1 and a worse one 0.5.)

Similar analysis on precancerous and normal cells yielded a maximum Youden index for the threshold of 108 for SI-AF1 particles (the sensitivity and specificity were 97% and 90%, respectively). The area under the ROC curve was 0.972. In the case of SI-AF2 particles, the maximum Youden index was obtained for the threshold of 110 (the sensitivity and specificity were 97% and 93%, respectively). The area under the ROC curve was 0.986. The extended statistics of the ROC curves is shown in Table S2 in the Supplementary Materials.

As discussed in the Background section, the sensitivity of currently used cytological tests **(**Pap smear and liquid-based cytology) for cervical carcinoma range from 16% to 82%. When detecting precancerous cervical lesions, the mean sensitivity was only 47% (range 30 - 80%). The specificity of Pap smear and liquid-based cytology is typically high, 95%.[48] The HPV-DNA screening is also reported to achieve similar specificity, while sensitivity can reach 80%.[49] Thus, the particle method described here shows the potential for substantially higher sensitivity with a comparable specificity. Clinical studies are now needed to determine the sensitivity and specificity of the folite particle-based method in patients.

Supplementary Material

Refer to Web version on PubMed Central for supplementary material.

Acknowledgments

Human tissue was obtained from the Cooperative Human Tissue Network.

Funding for this work from the National Science Foundation NSF CBET 1242214 (I.S.) and the National Cancer Institute 1R15CA126855-01 (C.W) are acknowledged.

References

1. Walboomers JMM, Jacobs MV, Manos MM, Bosch FX, Kummer JA, Shah KV, Snijders PJF, Peto J, Meijer CJLM, Muñoz N. Human papillomavirus is a necessary cause of invasive cervical cancer worldwide. The Journal of Pathology. 1999; 189:12–19. [PubMed: 10451482]
2. Nuovo J, Melnikow J, Howell LP. New tests for cervical cancer screening. Am Fam Physician. 2001; 64:780–786. [PubMed: 11563569]
3. Mitchell MF, Cantor SB, Ramanujam N, Tortolero-Luna G, Richards-Kortum R. Fluorescence spectroscopy for diagnosis of squamous intraepithelial lesions of the cervix. Obstetrics and Gynecology. 1999; 93:462–470. [PubMed: 10075001]
4. Monsonego J, Bosch FX, Coursaget P, Cox JT, Franco E, Frazer I, Sankaranarayanan R, Schiller J, Singer A, Wright T, Kinney W, Meijer C, Linder J. Cervical cancer control, priorities and new directions. International Journal of Cancer. 2004; 108:329–333.
5. Katki HA, Wentzensen N. How might hpv testing be integrated into cervical screening? Lancet Oncol. 2012; 13:8–10. [PubMed: 22177578]
6. Belinson JL, Pretorius RG, Zhang WH, Wu LY, Qiao YL, Elson P. Cervical cancer screening by simple visual inspection after acetic acid. Obstetrics and Gynecology. 2001; 98:441–444. [PubMed: 11530126]
7. Bhatla N, Mukhopadhyay A, Joshi S, Kumar A, Kriplani A, Pandey RM, Verma K. Visual inspection for cervical cancer screening: Evaluation by doctor versus paramedical worker. Indian journal of cancer. 2004; 41:32–6. [PubMed: 15105577]
8. Drezek RA, Collier T, Brookner CK, Malpica A, Lotan R, Richards-Kortum RR, Follen M. Laser scanning confocal microscopy of cervical tissue before and after application of acetic acid. American Journal of Obstetrics and Gynecology. 2000; 182:1135–1139. [PubMed: 10819847]
9. Pitris C, Goodman A, Boppart SA, Libus JJ, Fujimoto JG, Brezinski ME. High-resolution imaging of gynecologic neoplasms using optical coherence tomography. Obstetrics and Gynecology. 1999; 93:135–139. [PubMed: 9916971]
10. Iyer KS, Gaikwad RM, Woodworth CD, Volkov DO, Sokolov I. Physical labeling of papillomavirus-infected, immortal, and cancerous cervical epithelial cells with fluorescent silica beads. Cell Biochemistry and Biophysics. 2012; 63:109–116. [PubMed: 22351422]
11. Iyer S, Woodworth CD, Gaikwad RM, Kievsky YY, Sokolov I. Towards nonspecific detection of malignant cervical cells with fluorescent silica beads. Small. 2009; 5:2277–2284. [PubMed: 19415648]
12. Low PS, Henne WA, Doorneweerd DD. Discovery and development of folic-acid-based receptor targeting for imaging and therapy of cancer and inflammatory diseases. Acc Chem Res. 2007; 41:120–129. [PubMed: 17655275]
13. Sittig C, Hahner G, Marti A, Textor M, Spencer ND, Hauert R. The implant material, ti6al7nb: Surface microstructure, composition and properties. Journal of Materials Science-Materials in Medicine. 1999; 10:191–198. [PubMed: 15348150]
14. Santra S, Liesenfeld B, Dutta D, Chatel D, Batich CD, Tan W, Moudgil BM, Mericle RA. Folate conjugated fluorescent silica nanoparticles for labeling neoplastic cells. J Nanosci Nanotechnol. 2005; 5:899–904. [PubMed: 16060150]

15. Zhang HW, Sun ZG, Zhang SY, Han BS, Shen BG, Tung IC, Chin TS. Intergrain exchange coupling and coercivity mechanism of nanocrystalline sm2fe15-xcuxsi2c (x=0 and 1) ribbons prepared by melt spinning. Phys Rev B. 1999; 60:64–67.
16. Landmark KJ, Dimaggio S, Ward J, Kelly C, Vogt S, Hong S, Kotlyar A, Myc A, Thomas TP, Penner-Hahn JE, Baker JR, Holl MMB, Orr BG. Synthesis, characterization, and in vitro testing of superparamagnetic iron oxide nanoparticles targeted using folic acid-conjugated dendrimers. ACS Nano. 2008; 2:773–783. [PubMed: 19206610]
17. Wang Y, Xu J, Xia X, Yang M, Vangveravong S, Chen J, Mach RH, Xia Y. Sv119-gold nanocage conjugates: A new platform for targeting cancer cells via sigma-2 receptors. Nanoscale. 2012
18. Benezra M, Penate-Medina O, Zanzonico PB, Schaer D, Ow H, Burns A, Destanchina E, Longo V, Herz E, Iyer S, Wolchok J, Larson SM, Wiesner U, Bradbury MS. Multimodal silica nanoparticles are effective cancer-targeted probes in a model of human melanoma. The Journal of Clinical Investigation. 2011; 121:2768–2780. [PubMed: 21670497]
19. Wang S, Low PS. Folate-mediated targeting of antineoplastic drugs, imaging agents, and nucleic acids to cancer cells. J Controlled Release. 1998; 53:39–48.
20. Low PS, Antony AC. Folate receptor-targeted drugs for cancer and inflammatory diseases. Adv Drug Deliv Rev. 2004; 56:1055–1058. [PubMed: 15094205]
21. Sun C, Sze R, Zhang M. Folic acid-peg conjugated superparamagnetic nanoparticles for targeted cellular uptake and detection by mri. Journal of Biomedical Materials Research Part A. 2006; 78A: 550–557. [PubMed: 16736484]
22. Rosenholm JM, Meinander A, Peuhu E, Niemi R, Eriksson JE, Sahlgren C, Linden M. Targeting of porous hybrid silica nanoparticles to cancer cells. ACS Nano. 2009; 3:197–206. [PubMed: 19206267]
23. Lavi Y, Gov N, Edidin M, Gheber LA. Lifetime of major histocompatibility complex class-i membrane clusters is controlled by the actin cytoskeleton. Biophys J. 2012; 102:1543–50. [PubMed: 22500754]
24. Boyle S, Kolin DL, Bieler JG, Schneck JP, Wiseman PW, Edidin M. Quantum dot fluorescence characterizes the nanoscale organization of t cell receptors for antigen. Biophys J. 2011; 101:L57–9. [PubMed: 22261075]
25. Sokolov I, Naik S. Novel fluorescent silica nanoparticles: Towards ultrabright silica nanoparticles. Small. 2008; 4:934–939. [PubMed: 18581411]
26. Sokolov I, Kievsky YY, Kaszpurenko JM. Self-assembly of ultrabright fluorescent silica particles. Small. 2007; 3:419–423. [PubMed: 17245779]
27. Cho EB, Volkov DO, Sokolov I. Ultrabright fluorescent silica mesoporous silica nanoparticles: Control of particle size and dye loading. Adv Funct Mater. 2011:n/a–n/a.
28. Vallant T, Brunner H, Mayer U, Hoffmann H, Leitner T, Resch R, Friedbacher G. Formation of self-assembled octadecylsiloxane monolayers on mica and silicon surfaces studied by atomic force microscopy and infrared spectroscopy. Journal of Physical Chemistry B. 1998; 102:7190–7197.
29. Palantavida S, Guz NV, Sokolov I. Functionalized ultrabright fluorescent mesoporous silica nanoparticles. submitted.
30. Jaetao JE, Butler KS, Adolphi NL, Lovato DM, Bryant HC, Rabinowitz I, Winter SS, Tessier TE, Hathaway HJ, Bergemann C, Flynn ER, Larson RS. Enhanced leukemia cell detection using a novel magnetic needle and nanoparticles. Cancer Res. 2009; 69:8310–8316. [PubMed: 19808954]
31. Sanborn, WR.; Heuck, CC.; El Aouad, R.; Storch, WB. Fluorescence microscopy for disease diagnosis and environmental monitoring. World Health Organization; Regional Office for the Eastern Mediterranean, Cairo: 2005.
32. Wright, TC.; Ronnett, BM.; Kurman, RJ.; Ferenczy, A. Precancerous lesions of the cervix. In: Kurman, RJ., editor. Blaustein's pathology of the female genital tract. Springer-Verlag; New York: 1994.
33. Song S, Liem A, Miller JA, Lambert PF. Human papillomavirus types 16 e6 and e7 contribute differently to carcinogenesis. Virology. 2000; 267:141–150. [PubMed: 10662610]
34. Woodworth CD, Doniger J, Dipaolo JA. Immortalization of human foreskin keratinocytes by various human papillomavirus dnas corresponds to their association with cervical carcinoma. J Virol. 1989; 63:159–64. [PubMed: 2462058]

35. Woodworth CD, Waggoner S, Barnes W, Stoler MH, Dipaolo JA. Human cervical and foreskin epithelial cells immortalized by human papillomavirus dnas exhibit dysplastic differentiation in vivo. Cancer Res. 1990; 50:3709–15. [PubMed: 1692766]
36. Woodworth CD, Mcmullin E, Iglesias M, Plowman GD. Interleukin-1-alpha and tumor- necrosis-factor-alpha stimulate autocrine amphiregulin expression and proliferation of human papillomavirus-immortalized and carcinoma-derived cervical epithelial-cells. Proc Nat Acad Sci USA. 1995; 92:2840–2844. [PubMed: 7708734]
37. Cho EB, Volkov DO, Sokolov I. Ultrabright fluorescent silica mesoporous silica nanoparticles: Control of particle size and dye loading. Advanced Functional Materials. 2011; 21:3129–3135.
38. Cho EB, Volkov DO, Sokolov I. Ultrabright fluorescent mesoporous silica nanoparticles. Small. 2010; 6:2314–2319. [PubMed: 20859948]
39. Chithrani BD, Ghazani AA, Chan WCW. Determining the size and shape dependence of gold nanoparticle uptake into mammalian cells. Nano Lett. 2006; 6:662–668. [PubMed: 16608261]
40. Samuels, ML.; Witmer, JA. Statistics for the life sciences. Prentice Hall, Inc.; New Jersey: 1999.
41. Zou KH, Hall WJ, Shapiro DE. Smooth non-parametric receiver operating characteristic (roc) curves for continuous diagnostic tests. Stat Med. 1997; 16:2143–2156. [PubMed: 9330425]
42. Seong Ho Park JMG, Chan-Hee Jo. Receiver operating characteristic (roc) curve: Practical review for radiologists. Korean J Radiol. 2004; 5:11–18. [PubMed: 15064554]
43. Karpov I, Belcher RW, Linn JH. Electric force microscopy as a probe of active and passive elements of integrated circuits. Applied Surface Science. 1998; 125:332–338.
44. Abe M, Sugawara Y, Sawada K, Andoh Y, Morita S. Near-field optical imaging using force detection with new tip-electrode geometry. Applied Surface Science. 1999; 140:383–387.
45. Noel T, Franceschi S, Perez E, Vicendo P, Rico-Lattes I. High compacted DNA-polymer complexes via new polynorbornene polycationic latexes with acetate counterion. Langmuir. 2000; 16:8980–8983.
46. Vallhov H, Gabrielsson S, Strømme M, Scheynius A, Garcia-Bennett AE. Mesoporous silica particles induce size dependent effects on human dendritic cells. Nano Lett. 2007; 7:3576–3582. [PubMed: 17975942]
47. Rejman J, Oberle V, Zuhorn IS, Hoekstra D. Size-dependent internalization of particles via the pathways of clathrin and caveolae-mediated endocytosis. Biochem J. 2004; 377:159–169. [PubMed: 14505488]
48. Nanda K, Mccrory DC, Myers ER, Bastian LA, Hasselblad V, Hickey JD, Matchar DB. Accuracy of the papanicolaou test in screening for and follow-up of cervical cytologic abnormalitiesa systematic review. Annals of Internal Medicine. 2000; 132:810–819. [PubMed: 10819705]
49. Kuhn L, Denny L, Pollack A, Lorincz A, Richart RM, Wright TC. Human papillomavirus DNA testing for cervical cancer screening in low-resource settings. Journal of the National Cancer Institute. 2000; 92:818–825. [PubMed: 10814677]

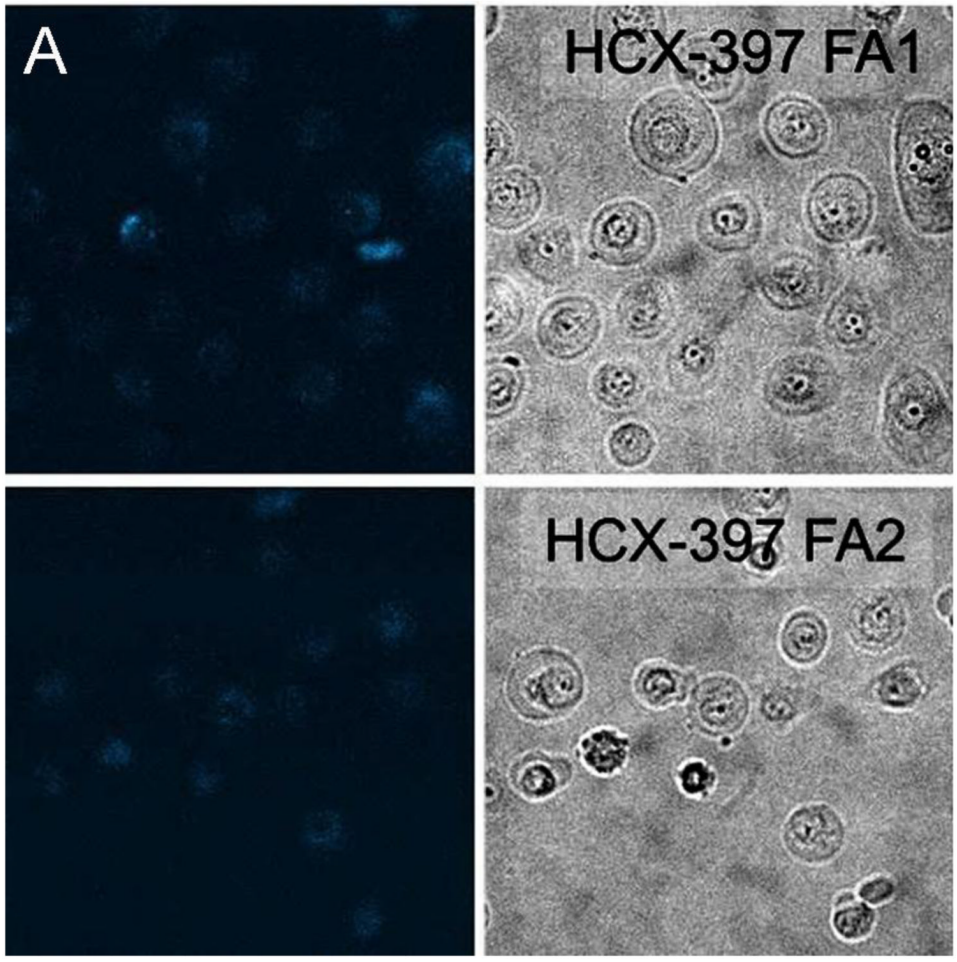

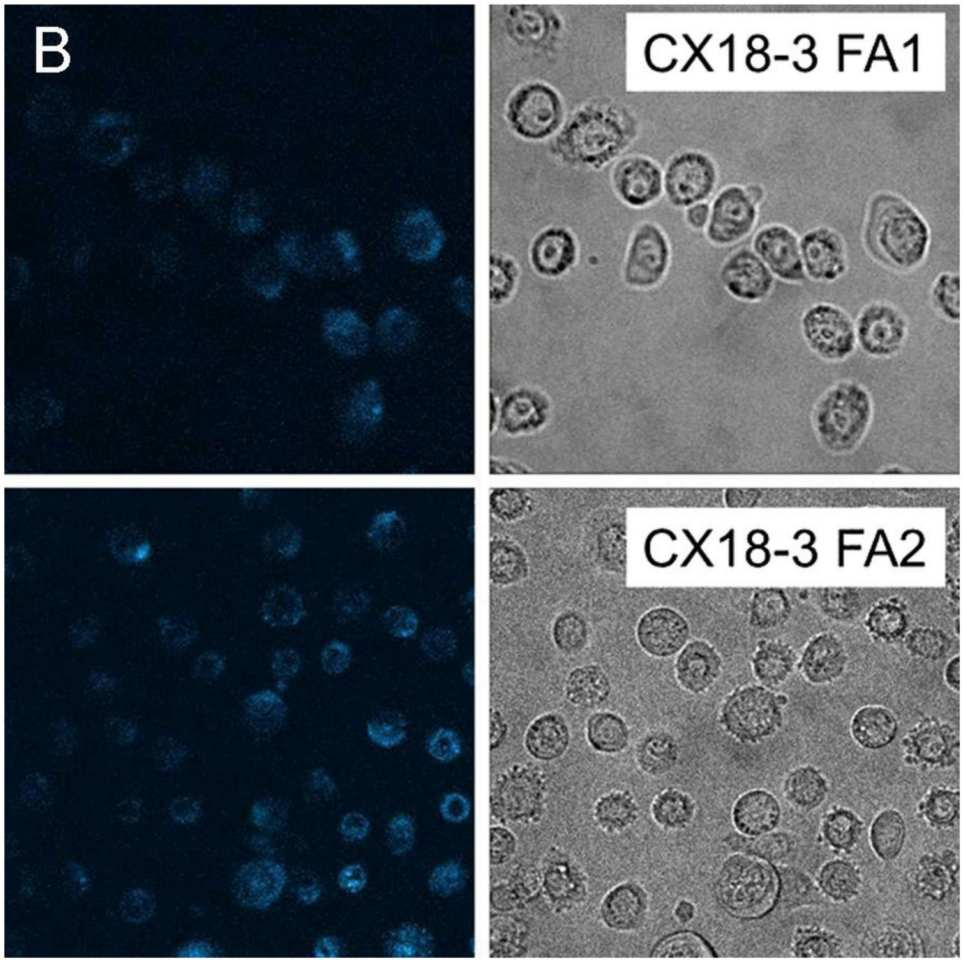

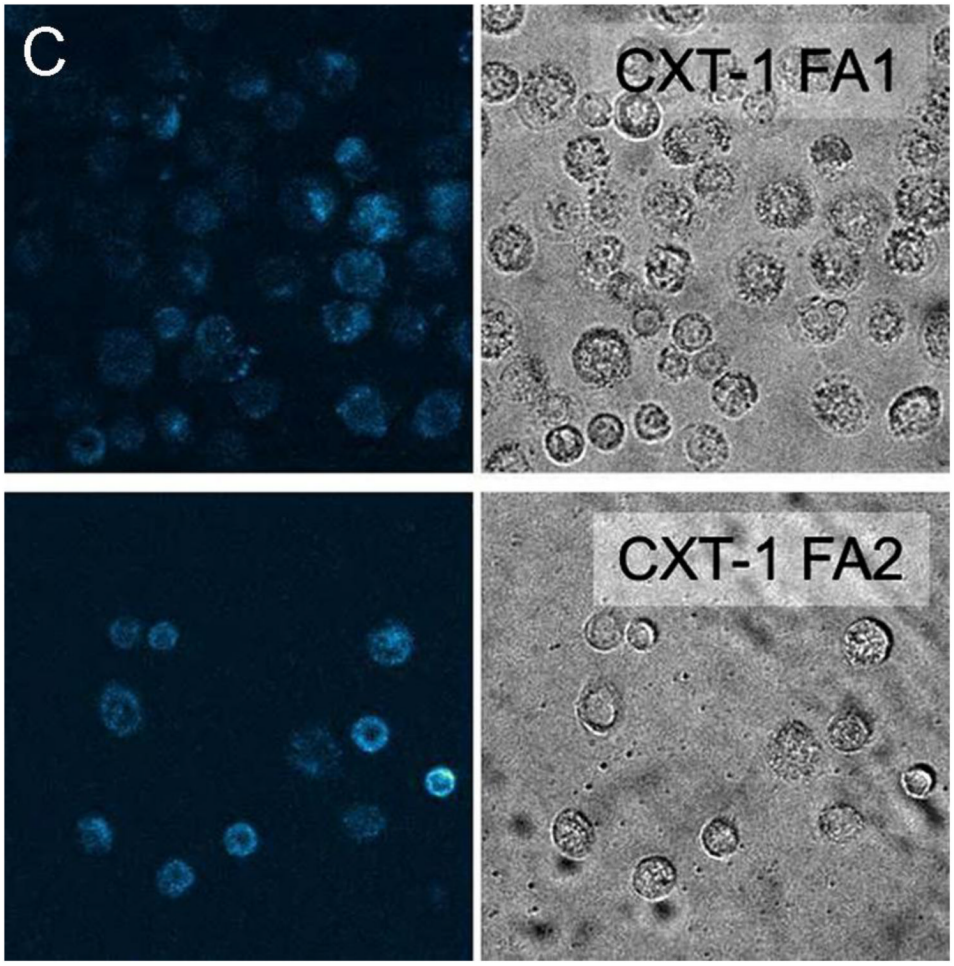

Figure 1.
Representative fluorescent images along with the corresponding bright field images of (A) normal, (B) precancerous/immortal, and (C) cancer cells obtained after incubation with SI-AF1 and SI-AF2 nanoparticles.

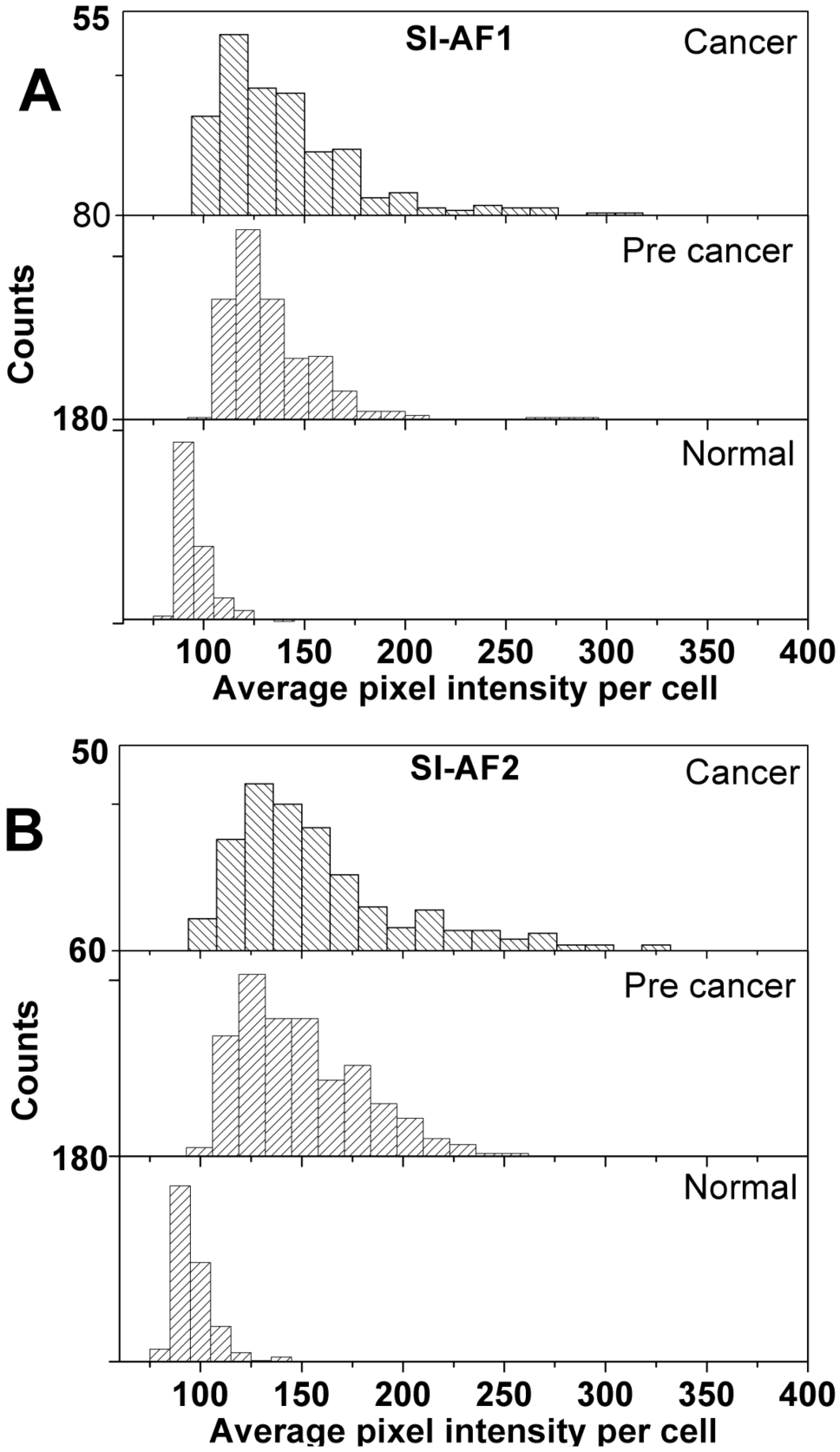

Figure 2.

Histograms of average pixel intensities per cell for the normal, precancerous, and cancerous cell cultures incubated with (A) SI-AF1 and (B) SI-AF2 particles.

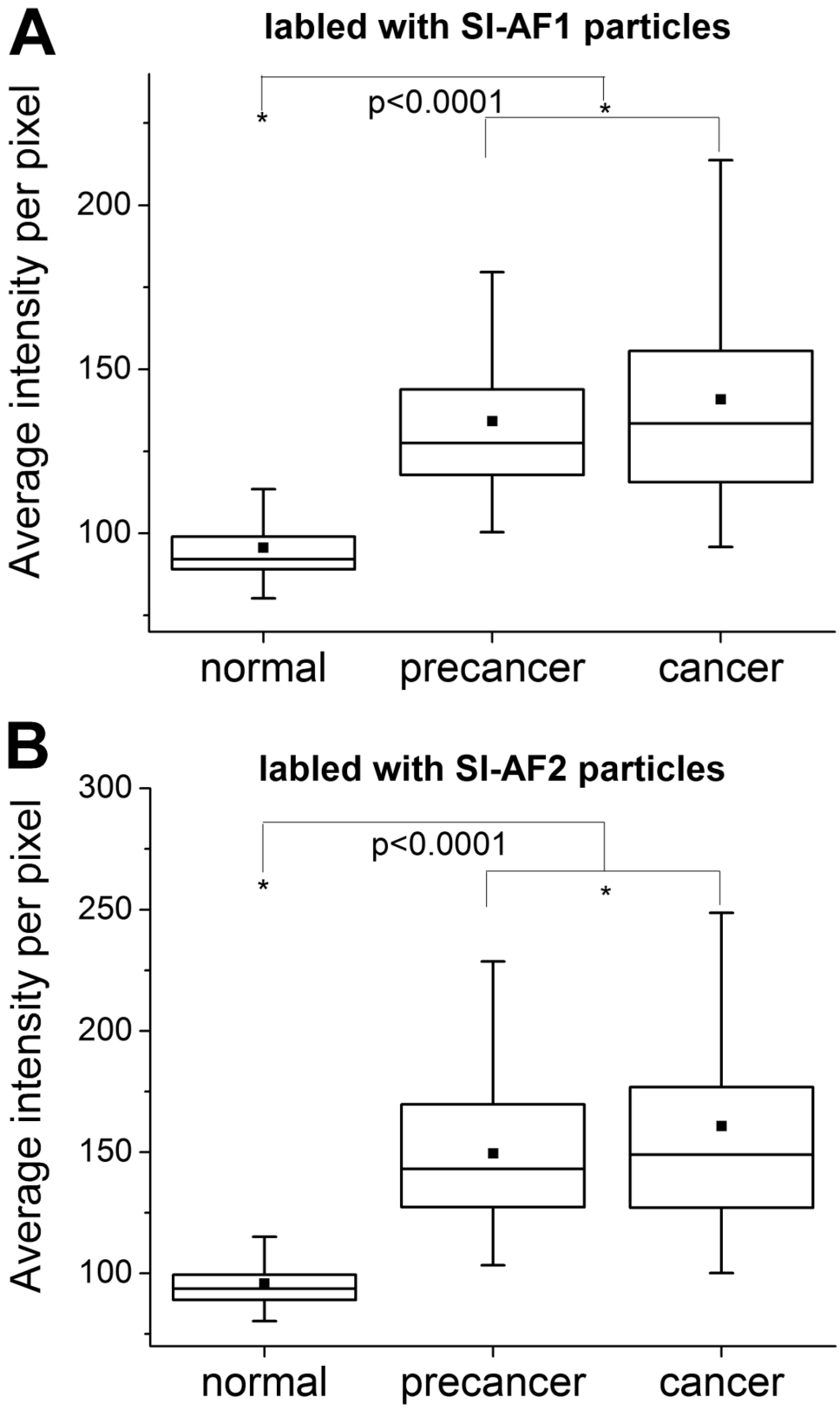

Figure 3.

Box plots of average pixel intensities per cell for the normal, precancerous, and cancerous cell cultures incubated with (A) SI-AF1 and (B) SI-AF2 particles. The 25/75% deviation, median, and mean are shown in the plots.

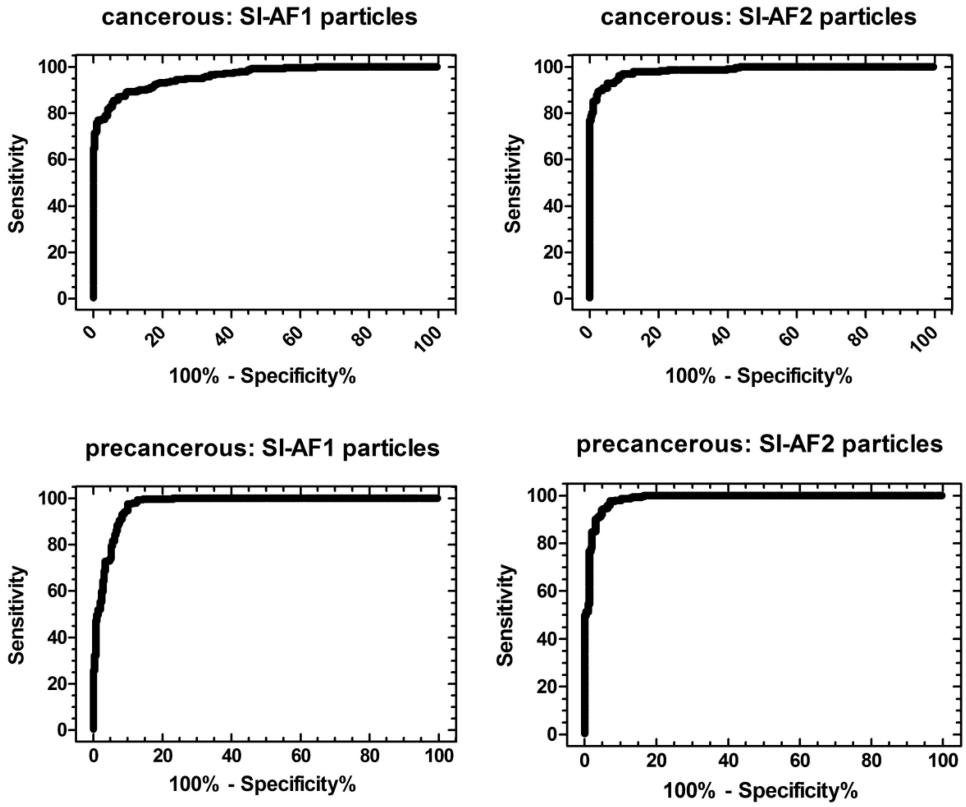

Figure 4.
The ROC curves calculated for cancer-normal and precancerous – normal groups of cells when using either SI-AF1 or SI-AF2 particles for the cell labeling.

Table 1

The results of Mann Whitney U tests comparing average pixel intensity distributions obtained for cancer, normal, and precancerous.

	Mann Whitney U tests		
		U	**p<**
SI-AF1			
	Cancer-Normal	3360	0.0001
	Normal-Precancerous	2450	0.0001
	Precancerous-Cancer	41700	0.16
SI-AF2			
	Cancer-Norm al	13 00	0.00 01
	Normal-Precancerous	1210	0.0001
	Precancerous-Cancer	40500	0.041